Experiments on the Parallel Hall Effect in Three-Dimensional Metamaterials

Christian Kern,[1,2] Vittoria Schuster,[1] Muamer Kadic,[1,2,3] and Martin Wegener[1,2]
[1]Institute of Applied Physics, Karlsruhe Institute of Technology (KIT), 76128 Karlsruhe, Germany
[2]Institute of Nanotechnology, Karlsruhe Institute of Technology (KIT), 76021 Karlsruhe, Germany
[3]Institut FEMTO-ST, CNRS, Université de Bourgogne Franche-Comté, 25000 Besançon, France
(Received 27 January 2017; published 3 April 2017)

The classical Hall effect in ordinary isotropic conducting materials describes the occurrence of a voltage perpendicular to the direction of the electric-current flow and perpendicular to the imposed magnetic-field vector. The Hall effect is routinely used in magnetic-field sensors. Here, we fabricate and characterize microstructured anisotropic metamaterials composed of a single semiconducting constituent (*n*-type ZnO) for which the direction and the sign of the Hall electric field can be tailored by microstructure. This class of metamaterials includes the possibility of a Hall voltage parallel—rather than perpendicular—to the magnetic-field vector. One possible future application arising from this far-reaching control of the effective electric-conductivity tensor is a sensor measuring the circulation of a magnetic field.

DOI: 10.1103/PhysRevApplied.7.044001

I. INTRODUCTION

The classical electrical Hall effect [1], the classical dynamical Hall effect (or the photon-drag effect) [2,3], the classical spin Hall effect [4,5], the quantum Hall effect [6], the fractional quantum Hall effect [7,8], the quantum spin Hall effect [9,10], the optical spin Hall effect [11–13], and the quantum spin Hall effect of light [14] are established phenomena. They are used in various applications, such as magnetic-field sensors [15], infrared light detectors [3], and resistance standards [6].

In the textbook discussion of the ordinary classical electrical (perpendicular) Hall effect [16], the magnetic component of the Lorentz force acts upon charged carriers in an isotropic conductor. As usual, this force is perpendicular to the velocity vector $\vec{v} = (v_x, 0, 0)^T$ of the carriers and perpendicular to the imposed magnetic-field vector $\vec{B} = (0, 0, B_z)^T$. As a result, the charges Q build up until the total Lorentz force is zero in the steady state, i.e., $\vec{F} = Q(\vec{E} + \vec{v} \times \vec{B}) = \vec{0}$. The corresponding perpendicular Hall electric field $\vec{E} = (0, E_y, 0)^T$ leads to a Hall voltage given by [16]

$$U_H^y = U_y = A_H I_x B_z / L_z, \tag{1}$$

where I_x is the imposed electric current, $A_H = 1/\rho$ the Hall coefficient (given by the inverse of the positive or negative charge density ρ of mobile carriers), and L_z the extent of the cuboid sample along the z direction [see Fig. 1(a)]. Ideally, the other sample dimensions L_x and L_y do not enter into the Hall voltage. However, for realistic samples, edge effects can play a role and small corrections may apply [15].

In this paper, we present experiments on anisotropic three-dimensional artificial materials (or metamaterials) exhibiting what we call the "parallel classical Hall effect." Here, the modified Hall voltage is given, rather, by

$$U_H^z = U_z = A_H^{\text{eff}} I_x B_z / L_y. \tag{2}$$

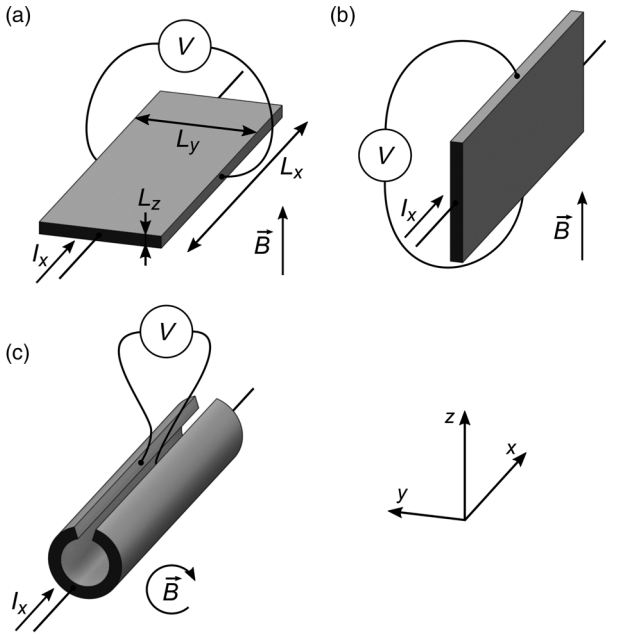

FIG. 1. (a) Illustration of the usual (perpendicular) classical Hall effect. A constant current I_x is injected along the x direction and a static magnetic field is applied along the z direction, i.e., $\vec{B} = (0, 0, B_z)^T$. As the Hall voltage U_H is proportional to $1/L_z$, thin platelets with $L_x > L_y \gg L_z$ are commonly used. (b) Unusual parallel Hall effect. Here, the Hall voltage is rather proportional to $1/L_y$, leading to the choice $L_x > L_z \gg L_y$. (c) Wrapped-up version of the geometry shown in (b). Here, the Hall voltage is proportional to the circulation of the magnetic field.

The usual perpendicular and the unusual parallel Hall effect are illustrated in Figs. 1(a) and 1(b), respectively. Note that the usual Hall voltage scales $\propto 1/L_z$, whereas the unusual Hall voltage scales $\propto 1/L_y$. The usual perpendicular Hall effect is commonly employed in commercially available devices to measure magnetic-field components B_z that are homogeneous on the scale of the Hall bar. The unusual parallel Hall effect could, for example, be used to measure the circulation of a magnetic field. To accomplish this task, one can adiabatically transform the Hall bar in Fig. 1(b) to the shape of an almost-closed ring in Fig. 1(c). The voltage picked up at the ends of this split ring would then be the line integral of the local Hall electric-field vector (which is proportional to the local magnetic-field vector) along the ring.

In such a device, the current I_x leads to an additional magnetic field, which, in principle, can influence the measured Hall voltage. However, any such contribution scales as I_x^2, whereas the actual Hall voltage scales as I_x. Similar effects are known from conventional Hall devices, where they can usually be neglected [15]. The sensitivity of a corresponding sensor is, as in the case of a conventional Hall sensor [15], mainly determined by the Hall coefficient and the Hall mobility of the constituent material. For the metamaterial structures introduced below, one expects an increase in current-related sensitivity and a decrease in voltage-related sensitivity compared to bulk material.

II. DESIGN

A few years ago, Briane and Milton [17] asked whether such highly unusual anisotropic materials exist, in principle. To provide a constructive existence proof, they considered and homogenized analytically an artificial structure (or metamaterial) composed of three different ingredient materials. One ingredient was an isotropic conductor with a zero Hall coefficient. The second ingredient had the same conductivity but a large Hall coefficient. The third ingredient was a fictitious, extremely anisotropic material with the same conductivity along the x direction, a large conductivity within the y-z plane (in the same coordinate system as above), and a zero Hall coefficient. More recently, inspired by our own work [18] on sign reversal of the isotropic Hall coefficient and supported by extensive numerical calculations, we simplified this suggestion to a metamaterial composed of only a single ordinary constituent material and the voids within [19]. Two possibilities have been considered, namely, structures made of either massive or hollow semiconducting rods. Here, we consider only hollow rods because this configuration is more easily amenable to advanced three-dimensional microfabrication [20]. Massive semiconducting rods have no conceptual advantage and would presently require a more demanding double-inversion fabrication procedure [21].

The blueprint for one unit cell of this metamaterial, as well as for an extended crystal based on a simple-cubic translational lattice with a lattice constant a, are shown in Fig. 2. As above, we consider a magnetic-field vector along

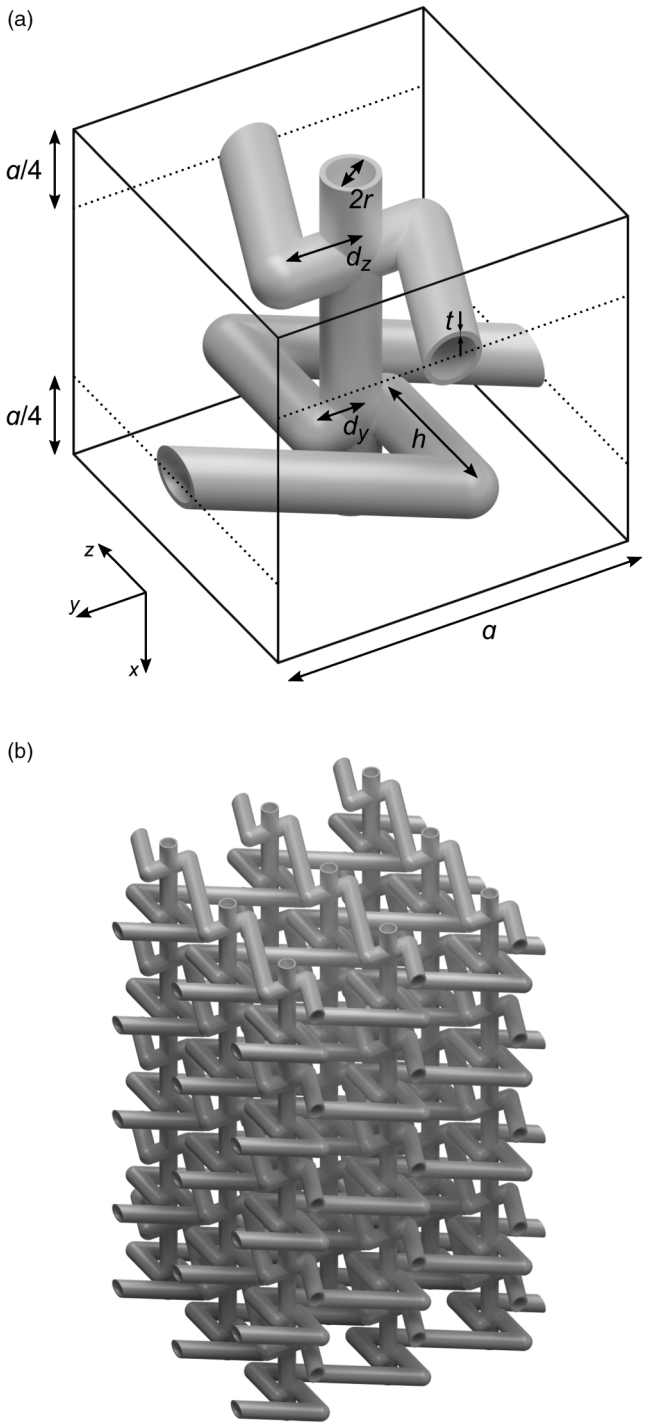

FIG. 2. (a) One unit cell of a metamaterial enabling the observation of the parallel Hall effect. (b) Extended part of a crystal based on a simple-cubic translational lattice with the lattice constant a. For the configuration shown, we have $d_y < 0$ and $d_z > 0$.

the z direction and a current flowing along the x direction. The structure has three different functional parts. Current is flowing through the straight hollow cylinders parallel to the x axis. The other two sets of hollow rods pick up the Hall voltage induced at the sides of the current-carrying hollow rods and guide it to the neighboring cells. In this fashion, the individual Hall-voltage sources are connected in series and a macroscopic Hall voltage along the y and/or z direction builds up. Depending on the signs of the geometrical displacement parameters d_y and d_z, which are defined in Fig. 2(a), the signs of the Hall voltages can be chosen. Clearly, the ordinary perpendicular Hall voltage becomes zero if one simply eliminates the connections with the separation parameter d_y. As pointed out previously [20], small absolute values of the lattice constant a are desirable because the resulting Hall voltage at fixed magnetic field B_z, fixed current I_x, fixed constituent material, and fixed number of unit cells along the three principal directions (i.e., $N_x = L_x/a$, $N_y = L_y/a$, and $N_z = L_z/a$) is inversely proportional to a. We thus consider microstructures rather than macroscopic lattices.

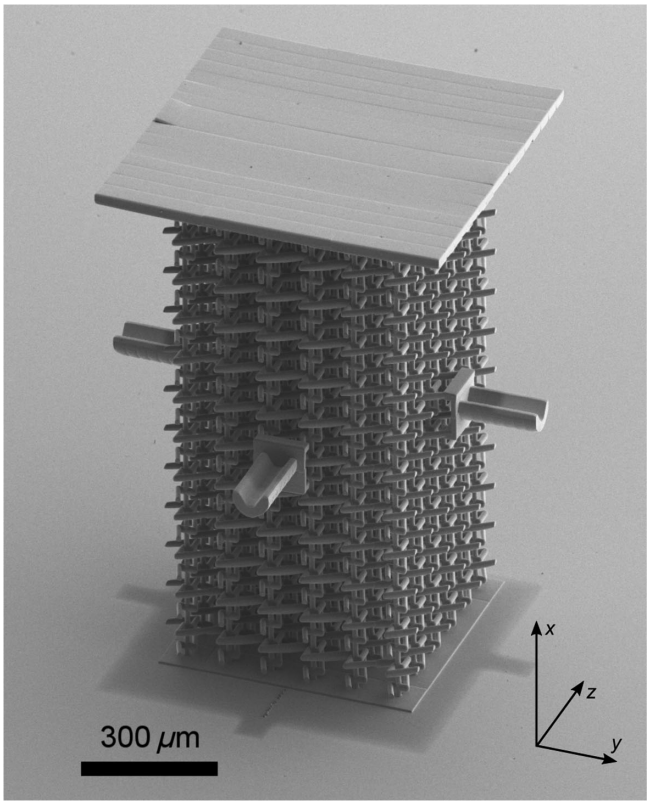

FIG. 3. Scanning electron micrograph of a fabricated structure after atomic-layer deposition and electron-beam evaporation. The shadow cast on the substrate by the top plate and the side contacts during electron-beam evaporation is clearly visible. The structure consists of $6 \times 6 \times 12$ unit cells. The design parameters are $a = 100\ \mu$m, $r = 6.25\ \mu$m, $h = 40\ \mu$m, $d_y = -10\ \mu$m, $d_z = 20\ \mu$m.

III. FABRICATION

The samples discussed in this paper are fabricated using a previously published three-step process [20], which is briefly summarized here: In a first step, we fabricate three-dimensional polymer structures on glass substrates using three-dimensional direct laser writing in a dip-in configuration [22]. We use a commercially available setup (Photonics Professional GT, Nanoscribe GmbH) and photoresist (IP-S, Nanoscribe GmbH). The polymer structures are electrically isolating (like air) and merely serve as a scaffold. In a second step, these polymer structures are coated conformally with a thin layer of n-type ZnO using atomic-layer deposition (Savannah 100, Cambridge Nanotech Inc.). The films are grown from water and diethylzinc at a temperature of 150 °C. Their thickness of $t = 185$ nm has been determined using ellipsometry on silicon-wafer substrates, which are coated together with the actual samples. In principle, one could use any semiconductor or metal. However, the atomic-layer deposition of n-type ZnO has become a well-established process during the past few years [23]. In order to obtain Ohmic contacts, we evaporate a bilayer of titanium and gold with thicknesses of 30 and 100 nm, respectively, using directional electron-beam evaporation in a third step. It is known that one can achieve low-resistivity Ohmic contacts on n-type ZnO using Ti/Au [24–26]. A polymer plate on top of the structures prevents the actual Hall element from being metal coated in this step as well. The four side contacts are intentionally protruding and are therefore partially metallized.

IV. MEASUREMENTS AND RESULTS

For the measurements under ambient conditions, we use a homebuilt probe station as in Ref. [20]. The magnetic field is imposed by a movable permanent magnet, which allows for measurements at positive, negative, and near-zero magnetic fields. The magnetic flux density at the sample location is $|B_z| = 0.83$ T. For imposing the current and measuring the Hall voltage, we use a source measurement unit (B2901A, Keysight Technologies, Inc.). Before the actual measurement, the contacts to the structure are made and the corresponding I-V curves are measured. The top of the structure and the substrate are contacted by tungsten needles for imposing the current I_x. Additionally, there are two pairs of opposing side contacts. Owing to the limited accessibility of the samples in the setup, only one pair is contacted in each measurement. From the two transverse voltages measured between each pair, we extract the two Hall voltages. As usual, unintentional additional asymmetries of the structure can lead to magnetic-field-independent offset voltages [20]. The Hall voltage is typically on the order of $100\ \mu$V at a current of $I_x = 0.5$ mA. Because of the fairly low Hall mobility of the atomic-layer-deposited thin ZnO films, the offset

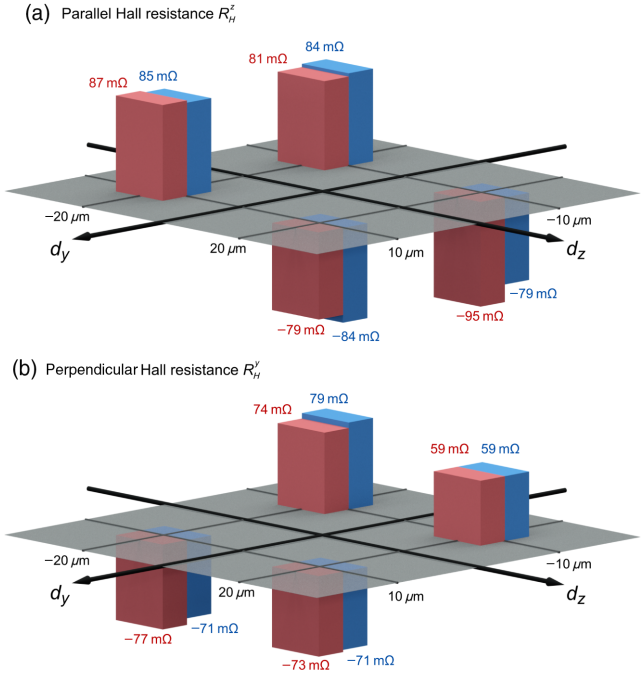

FIG. 4. (a) Measured parallel Hall resistance R_H^z and (b) perpendicular Hall resistance R_H^y versus the separation parameters d_y and d_z. The red and blue bars correspond to two different nominally identical sample sets. $B_z = 0.83$ T, $d_y = \pm 10$ μm, $d_z = \pm 20$ μm, and other parameters as in Fig. 3.

voltage is typically 10 times larger than the Hall voltage. Thus, the magnetic-field-independent offset voltages are subtracted by performing measurements at positive and negative magnetic fields B_z. We repeat these measurements for various current values I_x and find the expected proportional dependence $U_H = R_H I_x$. From fits to these raw data (not depicted, see Ref. [20]), we derive the perpendicular and the parallel Hall resistance.

Figure 4 shows the measured Hall resistances for metamaterial Hall bars with different values of d_y and d_z. First, R_H^z is finite, and hence there is a Hall voltage parallel to the magnetic field. The conventional perpendicular Hall voltages and resistances have a comparable modulus within the error bars. Both Hall resistances can be positive or negative depending on the geometry parameters. More precisely, the signs of d_y and d_z determine the signs of R_H^y and R_H^z, respectively.

Since the coating is an n-type semiconductor, a positive (negative) value of d_y leads to a negative (positive) value of R_H^y for a positive B_z. The same holds for d_z and R_H^z. The four sign combinations of the orthogonal and the parallel Hall voltage correspond to four different orientations of the Hall electric-field vector in the plane perpendicular to the direction of current flow.

One can tailor the parallel and orthogonal Hall voltages independently and continuously by adjusting the parameters d_y and d_z [19] and hence, in principle, realize any direction and magnitude of the corresponding Hall electric field in the x-y plane. Furthermore, it should also be possible to realize metamaterial structures exhibiting a parallel Hall effect independently of the orientation of the magnetic field in the y-z plane, i.e., perpendicular to the current flow [17].

V. ANALYTICAL MODEL

We have previously discussed numerical calculations [19]. It is thus more interesting to provide a simple analytical estimate of the Hall resistances for the structures studied here. We start by considering one of the current-carrying hollow cylinders oriented along the x axis in Fig. 2 and assume it is infinitely long. A cross section is illustrated in Fig. 5. Under steady-state conditions, the total Lorentz force within the y-z plane has to be zero. Assuming a homogeneous charge density ρ and current density j_x^{cyl}, with $I_x^{\mathrm{cyl}} = j_x^{\mathrm{cyl}} \pi[(r+t)^2 - r^2)]$ within the cylinder wall, the electric-field components E_y and E_z can be computed.

Performing the line integral of the electric-field vector from one black dot in Fig. 5 to the other side along the path indicated by the half circle, we obtain the voltage between the two black dots, i.e., the Hall voltage

$$U_H^{\mathrm{cyl}} = A_H I_x^{\mathrm{cyl}} B_z \frac{2}{\pi} \frac{r+t}{(r+t)^2 - r^2} \approx A_H I_x^{\mathrm{cyl}} B_z \frac{1}{t\pi}. \qquad (3)$$

The approximation given is valid for thin cylinder walls, i.e., in the limit $t \ll r$. Clearly, the result is equal to that for a Hall plate with thickness $L_z = t\pi$. On this basis, we can derive an expression for the Hall voltage of the entire structure. Here, we neglect any influence of the contacts and assume that the overall Hall voltage is simply given by the number of cells in series times the Hall voltage for a single hollow cylinder. For the perpendicular Hall voltage, N_y cells are wired up in series. For the parallel Hall voltage, N_z cells are connected in series. Furthermore, the current in one cylinder I_x^{cyl} in Eq. (3) is given by the total current I_x divided by the number of current-carrying cylinders of the Hall element in a plane normal to the x direction, i.e., $I_x^{\mathrm{cyl}} = I_x/(N_y N_z)$ (see Fig. 2).

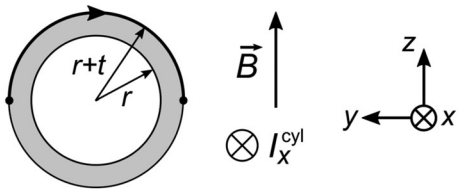

FIG. 5. Cross section of an infinitely long current carrying hollow cylinder (compare to Fig. 2) oriented along the x axis and subject to a static magnetic field $\vec{B}$ parallel to the z direction. This geometry results in a Hall voltage U_H^{cyl} between the two black dots on the cylinder sides. Adding up this voltage (3) for many unit cells in series allows us to formulate the metamaterial Hall resistances (4) and (5), respectively.

Provided that $|d_y|$ and $|d_z|$ are sufficiently large such that the hollow cylinders do not overlap (see Fig. 2), we obtain for the usual perpendicular and the unusual parallel Hall voltage, respectively,

$$U_H^y = \left(\mathrm{sgn}(d_y)\frac{1}{N_z}A_H B_z \frac{1}{t\pi}\right) I_x = R_H^y I_x \qquad (4)$$

and

$$U_H^z = \left(\mathrm{sgn}(d_z)\frac{1}{N_y}A_H B_z \frac{1}{t\pi}\right) I_x = R_H^z I_x. \qquad (5)$$

With $A_H^{\mathrm{eff}} = \mathrm{sgn}(d_z)A_H a/(t\pi)$, together with $N_y = L_y/a$ and $N_z = L_z/a$, we obtain formula (2) in the Introduction, with the scaling $\propto 1/L_y$. The wall thickness of $t = 185$ nm is determined by ellipsometry (see above). The Hall coefficient of $A_H = -2.5 \times 10^{-7}\,\mathrm{m^3\,C^{-1}}$ is determined by independent van der Pauw measurements on square-shaped samples (not depicted). Plugging these values, together with the experimentally quoted B_z, into the formulas, we obtain $|R_H^z| = |R_H^y| = 59$ mΩ. Considering the simplicity of the approach, these calculated values are in good agreement with the experimental ones summarized in Fig. 4. The signs of the resistances agree, too (compare to Fig. 4).

To avoid confusion, we note that the voltage sign conventions used here and in Ref. [19] do not agree. According to the sign convention used here, which is consistent with that in Ref. [20], an n-type material subject to a positive current and a positive magnetic field leads to a negative Hall voltage and a negative Hall resistance. In Ref. [19], the sign is flipped throughout.

VI. RESISTANCE VERSUS SAMPLE DIMENSIONS

The usual perpendicular Hall voltage and the unusual parallel Hall voltage have a distinct dependence on the sample dimensions (see also the Introduction). In a usual Hall plate, the measured Hall voltage is inversely proportional to the thickness L_z of the Hall plate in the direction of the magnetic field. In case of the unusual parallel Hall effect, the Hall voltage is inversely proportional to the sample thickness in the y direction, L_y, i.e., inversely proportional to the thickness in the direction perpendicular to the magnetic field [19].

In order to investigate these different scalings experimentally, we fabricate a set of samples corresponding to different values of N_y and determine their parallel Hall resistance as described above. As we are interested only in their parallel Hall voltage, we fabricate them with two side contacts only. Figure 6 exhibits the measured parallel Hall resistance versus the number of unit cells in the y direction, N_y, on a double-logarithmic scale. Measured Hall resistances from eight different samples are shown, of which four pairs are nominally identical. This repetition allows for studying the effect of fabrication errors. Clearly, the experimental results closely follow the expected $\propto N_y^{-1}$ behavior indicated by the straight line with slope -1.

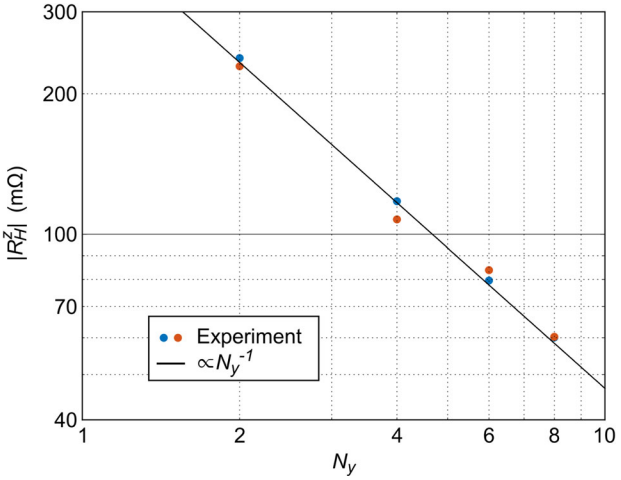

FIG. 6. Measured parallel Hall resistance $|R_H^z|$ versus N_y. For each N_y, two nominally identical samples (shown in red and blue) are fabricated. The two points for $N_y = 8$ coincide within the dot size. The black solid straight line with a slope of -1 in this double-logarithmic representation demonstrates the scaling according to $R_H^z \propto 1/N_y$. The parameters are $a = 100$ μm, $r = 6.25$ μm, $h = 40$ μm, $d_y = 10$ μm, $d_z = 20$ μm, $N_x = 12$, and $N_z = 6$.

VII. CONCLUSION

In this paper, we fabricate and characterize metamaterials composed of a single semiconductor material and air voids within which exhibit the parallel Hall effect. We also combine the unconventional parallel Hall effect with the conventional (perpendicular) Hall effect and realize four different sign combinations. Quite unlike the usual perpendicular Hall resistance, the measured parallel Hall resistance is inversely proportional to the number of unit cells perpendicular to the magnetic-field axis. The measured Hall resistances are in good agreement with a simple analytical model.

ACKNOWLEDGMENTS

We acknowledge support from the Karlsruhe School of Optics & Photonics (KSOP), the Hector Fellow Academy, the KIT Nanostructure Service Laboratory (NSL), and the Helmholtz Program Science and Technology of Nanosystems (STN).

C. K. and V. S. contributed equally to this work.

[1] E. H. Hall, On a new action of the magnet on electric currents, Am. J. Math. **2**, 287 (1879).

[2] H. M. Barlow, The application of the Hall effect in a semiconductor to the measurement of power in an electromagnetic field, Nature (London) **173**, 41 (1954).

[3] A. F. Gibson, M. F. Kimmitt, and A. C. Walker, Photon drag in germanium, Appl. Phys. Lett. **17**, 75 (1970).
[4] M. I. Dyakonov and V. I. Perel, Possibility of orienting electron spins with current, Sov. Phys. JETP Lett. **13**, 467 (1971).
[5] Q. Hao and G. Xiao, Giant Spin Hall Effect and Switching Induced by Spin-Transfer Torque in a $W/Co_{40}Fe_{40}B_{20}/MgO$ Structure with Perpendicular Magnetic Anisotropy, Phys. Rev. Applied **3**, 034009 (2015).
[6] K. v. Klitzing, G. Dorda, and M. Pepper, New Method for High-Accuracy Determination of the Fine-Structure Constant Based on Quantized Hall Resistance, Phys. Rev. Lett. **45**, 494 (1980).
[7] D. C. Tsui, H. L. Störmer, and A. C. Gossard, Two-Dimensional Magnetotransport in the Extreme Quantum Limit, Phys. Rev. Lett. **48**, 1559 (1982).
[8] R. B. Laughlin, Anomalous Quantum Hall Effect: An Incompressible Quantum Fluid with Fractionally Charged Excitations, Phys. Rev. Lett. **50**, 1395 (1983).
[9] C. L. Kane and E. J. Mele, Quantum Spin Hall Effect in Graphene, Phys. Rev. Lett. **95**, 226801 (2005).
[10] M. König, S. Wiedmann, C. Brüne, A. Roth, H. Buhmann, L. W. Molenkamp, X.-L. Qi, and S.-C. Zhang, Quantum spin Hall insulator state in HgTe quantum wells, Science **318**, 766 (2007).
[11] A. V. Kavokin, G. Malpuech, and M. M. Glazov, Optical Spin Hall Effect, Phys. Rev. Lett. **95**, 136601 (2005).
[12] C. Leyder, M. Romanelli, J. Ph. Karr, E. Giacobino, T. C. H. Liew, M. M. Glazov, A. V. Kavokin, G. Malpuech, and A. Bramati, Observation of the optical spin Hall effect, Nat. Phys. **3**, 628 (2007).
[13] X. Yin, Z. Ye, J. Rho, Y. Wang, and X. Zhang, Photonic spin Hall effect at metasurfaces, Science **339**, 1405 (2013).
[14] K. Y. Bliokh, D. Smirnova, and F. Nori, Quantum spin Hall effect of light, Science **348**, 1448 (2015).
[15] R. S. Popovic, *Hall Effect Devices* (Taylor & Francis, London, 2003).
[16] P. Yu and M. Cardona, *Fundamentals of Semiconductors* (Springer-Verlag, Berlin, 2010).
[17] M. Briane and G. W. Milton, An antisymmetric effective Hall matrix, SIAM J. Appl. Math. **70**, 1810 (2010).
[18] M. Kadic, R. Schittny, T. Bückmann, C. Kern, and M. Wegener, Hall-Effect Sign Inversion in a Realizable 3D Metamaterial, Phys. Rev. X **5**, 021030 (2015).
[19] C. Kern, M. Kadic, and M. Wegener, Parallel Hall effect from three-dimensional single-component metamaterials, Appl. Phys. Lett. **107**, 132103 (2015).
[20] C. Kern, M. Kadic, and M. Wegener, Experimental Evidence for Sign Reversal of the Hall Coefficient in Three-Dimensional Metamaterials, Phys. Rev. Lett. **118**, 016601 (2017).
[21] A. Frölich, J. Fischer, T. Zebrowski, K. Busch, and M. Wegener, Titania woodpiles with complete three-dimensional photonic bandgaps in the visible, Adv. Mater. **25**, 3588 (2013).
[22] T. Bückmann, N. Stenger, M. Kadic, J. Kaschke, A. Frölich, T. Kennerknecht, C. Eberl, M. Thiel, and M. Wegener, Tailored 3D mechanical metamaterials made by dip-in direct-laser-writing optical lithography, Adv. Mater. **24**, 2710 (2012).
[23] T. Tynell and M. Karppinen, Atomic layer deposition of ZnO: A review, Semicond. Sci. Technol. **29**, 043001 (2014).
[24] J.-J. Chen, S. Jang, T. J. Anderson, F. Ren, Y. Li, H.-S. Kim, B. P. Gila, D. P. Norton, and S. J. Pearton, Low specific contact resistance Ti/Au contacts on ZnO, Appl. Phys. Lett. **88**, 122107 (2006).
[25] L. J. Brillson and Y. Lu, ZnO Schottky barriers and Ohmic contacts, J. Appl. Phys. **109**, 121301 (2011).
[26] E. Guziewicz, M. Godlewski, L. Wachnicki, T. A. Krajewski, G. Luka, S. Gieraltowska, R. Jakiela, A. Stonert, W. Lisowski, M. Krawczyk, J. W. Sobczak, and A. Jablonski, ALD grown zinc oxide with controllable electrical properties, Semicond. Sci. Technol. **27**, 074011 (2012).